International Journal of Modern Physics A
Vol. 36, Nos. 11 & 12 (2021) 2140017 (13 pages)

DOI: 10.1142/S0217751X21400170

The impact of neutralizer-free ignition of a radio frequency ion thruster on the lifetime of the ion optics system

Long-Fei Ma, Li Duan,[*,§] Jian-Wu He[†,§] and Qi Kang[‡,§]

Center for Gravitational Wave Experiment, National Microgravity Laboratory, Institute of Mechanics, Chinese Academy of Sciences (CAS), Beijing 100190, China

Taiji Laboratory for Gravitational Wave Universe (Beijing/Hangzhou), University of Chinese Academy of Sciences (UCAS), Beijing 100049, China
[*]*duanli@imech.ac.cn*
[†]*javehe@imech.ac.cn*
[‡]*kq@imech.ac.cn*

[¶]*On behalf of The Taiji Scientific Collaboration*

Received 15 September 2020
Accepted 30 October 2020
Published 9 April 2021

In the initial stage of a radio frequency ion thruster (RIT) ignition, an influx of electrons is required from an external source into the discharge chamber and ionization of the neutral gas propellant. A neutralizer-free method for Townsend breakdown discharge ignition based on Paschen's law was developed in this study. The feasibility of the ignition method was confirmed by performing thousands of ignition experiments. Metallic Molybdenum (Mo), pyrolytic graphite (PG) and $Zr_{41.2}Ti_{13.8}Cu_{12.5}Ni_{10}Be_{22.2}$ alloy acceleration grids were prepared, and ignition-induced damage on the grids was investigated. A field-emission scanning electron microscope was used to inspect surface damage on the grids after multiple ignitions and to analyze the influence of the ignition method on the lifetime of the ion optical system. Grid materials for space missions that require multiple RIT ignitions (10^3) should be high-strength blocks that are resistant to sputtering corrosion and high temperature.

Keywords: Radio-frequency ion thruster; Townsend discharge; Paschen's law; neutralizer-free ignition; ion optical system.

1. 1. Introduction

In the 1960s, the University of Giessen took the lead in research on radio frequency ion thrusters (RITs), which are grid ion thrusters. After decades of development, Loeb *et al.*[1] manufactured a series of RITs. Since 2000, research teams in Britain,[2] the USA,[3–5] Japan,[6,7] Russia,[8] China[9–11] and other countries have optimized RIT structures and radio frequency (RF) plasma through experiment and simulation. However, few studies have focused on RIT ignition method and processes.

[§]Corresponding authors.
[¶]For more details, please refer to article 2102002 of this Special Issue.

Electrons for RIT ignition must be introduced to the discharge chamber from an external source, which has traditionally been the neutralizer.[12–14] Because of the positive potential of the RIT ion optical system, electrons ejected by the neutralizer are guided into the discharge chamber. Once the densities of the electrons and the neutral gas propellant reach a certain threshold, the electrons ionize the neutral particles, and the plasma discharge is sustained through the continuous absorption of RF energy.

Mistoco *et al*.[15] designed a new RIT ignition method based on Paschen's law. The electric potential difference between the two poles of RF antenna outside the discharge chamber resulted in the generation of a strong electric field. They used the electric field to breakdown the neutral gas propellant in the discharge chamber for thruster ignition. The plasma discharge was maintained during operation of the thruster by adjusting the propellant gas flow rate and the RF power. The RF module must provide a large initial RF power for this type of ignition, which is difficult to achieve in engineering. Busek[3] recently employed the pulsed high-voltage breakdown discharge of an ion optical system to ignite a RIT while supplying the propellant gas at a normal flow rate. The acceleration grid loaded instantly at the high voltage, and a strong electric field was generated between the acceleration and the screen grids. The propellant gas molecules between the grids generated a large number of electrons at the moment of breakdown. The electric field drove some of the electrons into the discharge chamber, which ionized the propellant gas. This generated additional electrons that were accelerated in the RF field to maintain the plasma discharge. However, the ignition method required an additional transformer circuit, which increased the complexity of the RF ion thruster system.

A new neutralizer-free RIT ignition method based on Townsend breakdown discharge and Paschen's law[16] was developed in this paper. Thousands of ignitions were performed to assess the feasibility of the ignition method. The common grid materials of ion thrusters of Molybdenum (Mo) and pyrolytic graphite (PG),[17] and a new $Zr_{41.2}Ti_{13.8}Cu_{12.5}Ni_{10}Be_{22.2}$ metal alloy[18–20] which has characteristics of high strength, high hardness and resistance to sputtering were used to prepare acceleration grids, and the grids were examined to investigate trends in ignition-induced damage in the different materials. The mechanisms and the evolution of damage on the materials surface were determined after multiple ignitions. Finally, the influence of the ignition method on the lifetime of the ion optical system and ignition limits was evaluated.

2. Methods

The principle of RIT is illustrated in Fig. 1. The mass flow controller is used to regulate the propellant gas flow rate with a high precision. The propellant gas flows through the gas inlet of the thruster into the discharge chamber. When the RF antenna loads RF current, an electromagnetic field is induced in the discharge chamber. Electrons are energized in the induced electric field and collide with neutral gas particles. Some of the gas particles ionize, giving rise to a self-sustained RF plasma discharge. Ions in the plasma are extracted and accelerated because of the electric potential difference between

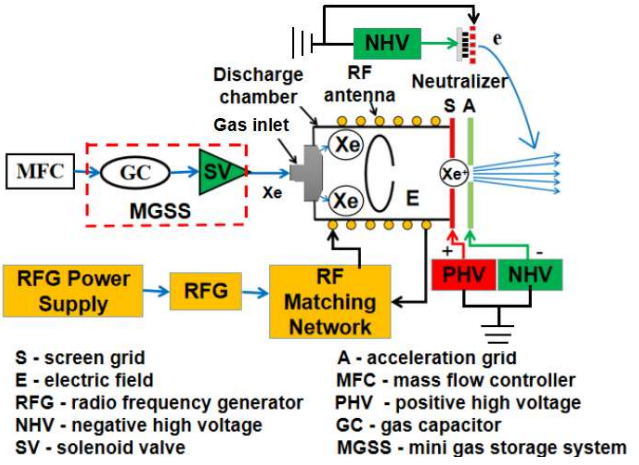

Fig. 1. μRIT-1 structure and operating principle.[21]

the plasma and the ion optical system, and generate effective thrust. The neutralizer emits electrons that neutralize the ion beam to maintain the electric neutrality of the RF ion propulsion system.

The research object of the ignition experiments was the ion optical system of μRIT-1 in this paper. The μRIT-1 system was designed for the Space Taiji Project in China, which will be launched for the detection of gravitational waves in space.

The μRIT-1 ion optical system had a two-grid structure (Fig. 2). The screen grid was made of metallic Mo with a thickness of 0.3 mm and five beam holes of 1.9 mm in diameter. Each acceleration grid was 1.0 mm thick with five beam holes of 1.2 mm in diameter. The grids were polished prior to assembly and then were set 0.7 mm apart to prevent discharge between them during operation of the thruster. The grid transparency Φ_s was based on the thrust range T of the RIT, which was calculated using the following equations[2]:

$$T = \frac{I_b M_i}{e}\sqrt{\frac{2e}{M_i}U_b}\ , \tag{1}$$

$$I_{b,\max} = \frac{4\varepsilon_0}{9}\sqrt{\frac{2q}{M_i}}\frac{V_T^{3/2}}{l_e^2}A_s\phi_s\,, \tag{2}$$

where $I_{b,\max}$ is the maximum ion beam transmission through the ion optical system, M_i is the mass of a propellant gas ion, e is the charge of the electron, U_b is the effective acceleration voltage, ε_0 is the permittivity of a vacuum, q is the ion charge, V_T is the electric potential difference between the grids, l_e is the effective grid distance and A_s is the effective area of the screen grid.

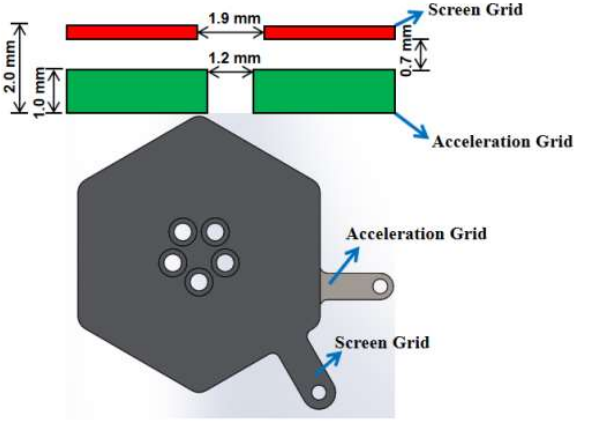

Fig. 2. The structure of the μRIT-1 ion optics system.

In neutralizer-free ignition, high-pressure gas pulses promote breakdown discharge between the grids within a desired voltage range via the Townsend breakdown discharge mechanism. Once breakdown discharge occurs, a large number of electrons are generated in an electron avalanche and enter the discharge chamber with guidance from the electric field. Propellant gas atoms collide with the electrons, and some of them ionize. Coupling with the RF power generates a self-sustained plasma in the discharge chamber.

Townsend breakdown discharge damage the surfaces of the grids. Studying damage on different grid materials caused by ignition is important from both scientific and engineering perspectives. Ion beam sputtering and corrosive beam holes in the acceleration grids are problematic, because the performance and ignition stability of the thruster will be adversely affected if the holes widen. This increases the risk of acceleration grid failure, so we evaluated the characteristics of acceleration grid damage in this paper. Mo and PG are common ion optical system materials that exhibit good electrical conductivity and mechanical properties. The $Zr_{41.2}Ti_{13.8}Cu_{12.5}Ni_{10}Be_{22.2}$ alloy is a new alloy material that also displays good electrical conductivity, thermal conductivity and other desirable properties.[18] The $Zr_{41.2}Ti_{13.8}Cu_{12.5}Ni_{10}Be_{22.2}$ alloy was used as an RIT acceleration grid for the first time in this study.

A small gas storage module was placed between the gas mass flow controller and the μRIT-1 gas inlet to study the Townsend breakdown discharge conditions, Paschen's law and the feasibility of using the ignition method with the μRIT-1 grids. The gas storage module included a gas capacitor and a solenoid valve and Xe was used as the gas propellant (Fig. 1). The gas propellant mass flow rate was set to 0.1 sccm to ignite the μRIT-1 and the pressure in the gas storage module was increased by closing the solenoid valve. When the solenoid valve opened, a gas pulse entered the discharge chamber and the ion optical system. The gas pressure between the grids was controlled by adjusting the solenoid valve closing time, and a pressure sensor was used to measure the actual gas pressure. Paschen' law was used to determine the breakdown discharge voltage of each

grid material on the basis of the distance between grids, the threshold voltage, and the gas pressure. After 1000 ignition, surface damage on each grid was examined using an S-4800 field-emission scanning electron microscope (Hitachi, Tokyo, Japan) at an emission voltage of 20.0 kV. An X-Max energy-dispersive X-ray spectrometer (Horiba, Kyoto, Japan) in conjunction with the scanning electron microscope was used to analyze the energy spectra of particles adhering to the grid surfaces and to identify the source of the particles.

3. Results

3.1. *Breakdown discharge conditions and feasibility of the ignition method*

On the basis of the Townsend breakdown discharge conditions and Paschen's law,[16] the threshold voltage V_{bd} required for breakdown discharge in the μRIT-1 ion optical system was governed by the distance d between the grids, the gas pressure p between the grids, the grid material, and the surface roughness of the grids. V_{bd} was calculated using the following equation:

$$V_{bd} = \frac{B \cdot pd}{\ln \frac{A \cdot pd}{\ln\left(1+1/\gamma\right)}}, \tag{3}$$

where γ is Townsend's second ionization coefficient, and A and B are the constants related to the gas species, 3.58 $cm^{-1}Torr^{-1}$ and -351.7 $V \cdot cm^{-1}$ $Torr^{-1}$ with Xe.

The three materials had different physical characteristics (Table 1), so the μRIT-1 acceleration grids had different appearances. The screen grid voltage ranged from 0 to 2 kV, and the acceleration grid was connected to the ground. The grids voltage was unloaded after ignition, and a mini dynamic gas pressure sensor (Kulite, USA) was used to measure the actual discharge gas pressure. The relationships between the threshold voltage, the distance d between the grids and the gas pressure p when d = 0.7 mm are shown in Fig. 3. The curves in Fig. 3 are consistent with discharge over short distance at low pressures according to Paschen's law. The γ in equation varied because the characteristics of the three materials differed. Thus, the threshold voltages of the μRIT-1 ion optical system varied, even at the same gas pressure.

Table 1. Physical properties of the materials.

	Density (g/cm^3)	Yield strength (MPa)	Melting point (℃)
Mo	10.2	650	2620
PG	2.1	83.6(ab) 320(c)	3520
$Zr_{41.2}Ti_{13.8}Cu_{12.5}Ni_{10}Be_{22.2}$	6.0	1900	1083

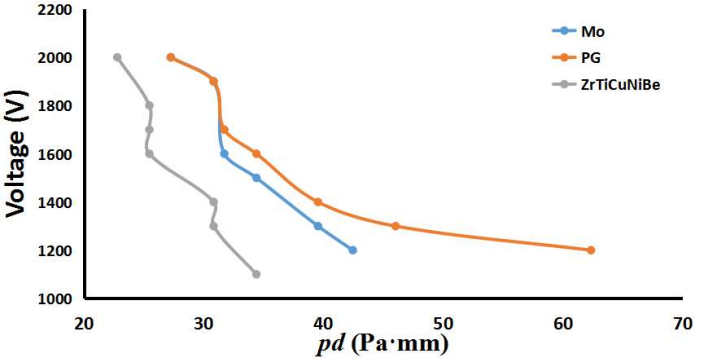

Fig. 3. Threshold voltage V curves plotted as a function of pd (p is the gas pressure; d is the distance between the grids).

The screen grid voltage was set to 1700 V for the experiment involving 1000 ignitions. On the basis of the discharge law, the gas pressure between the screen grid and the acceleration grids (Mo and PG) was held at 45.3 Pa, and the pressure between the screen and alloy grid was held at 36.4 Pa. Nearly, 100% of the μRIT-1 ignitions were successful and the thruster was operational after ignition.

3.2. *Damage on the molybdenum grid*

Scanning electron microscopy (SEM) images of the Mo acceleration grid surface (Fig. 4) were collected after 300, 500 and 1000 ignitions. A small number of hemispherical pits appeared on the surface of the gird after the first 300 ignitions (Fig. 4(a)). Their diameters ranged from several micrometers to 10 μm, and the pits were concentrated near the acceleration grid beam holes. After 500 ignitions, larger pits over 10 μm in diameter indicated collapse. Areas with laminar pre-damage and clear boundaries can be seen in Fig. 4(b). After 1000 ignitions, the gird surface exhibited bubbly-like bulges in clusters (Fig. 4(c_1)). The clusters merged into larger protrusions because of breakdown discharge in the ion optical system and the grid developed cracks. Once the cracks penetrated the protrusions, debris on the grid surface appeared to peel off in layers. A large proportion of the surface was damaged, as shown in Figs. 4(c_2) and 4(c_3). The shed debris was concentrated near the grid beam holes in Fig. 4(c_4), which indicated that breakdown discharge occurred in this section of the grid.

Numerous microparticles can be seen adhering to the surface of the Mo acceleration grid in the SEM images. Energy-dispersive X-ray spectroscopy (EDS) analysis of selected particles indicated that they contained mostly Mo in Fig. 5. This indicated that the particles were generated as the surface of the grid was damaged during breakdown discharge in the ion optical system. The temperature increased immediately in areas that were impacted by breakdown discharge, which melted the material. The material fell from the surface in the form of molten particles that adhered to the surface of the grid.

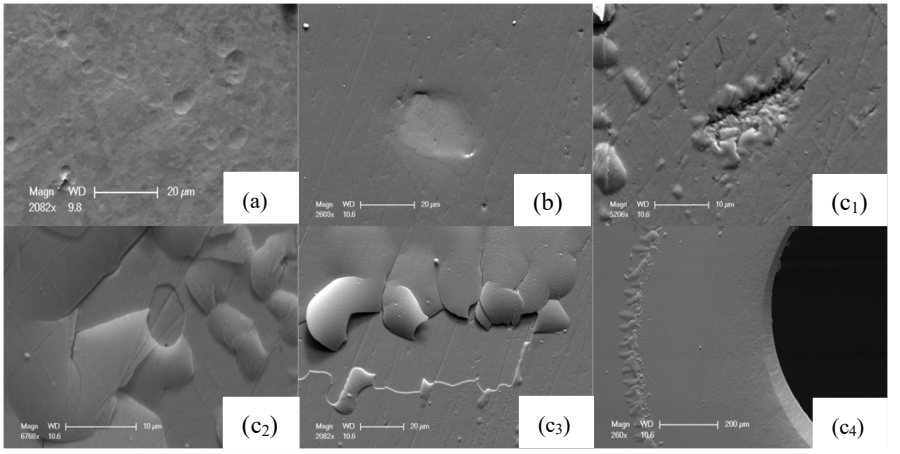

Fig. 4. The evolution of surface damage on the Mo grid observed after (a) 300, (b) 500 and (c) 1000 ignitions.

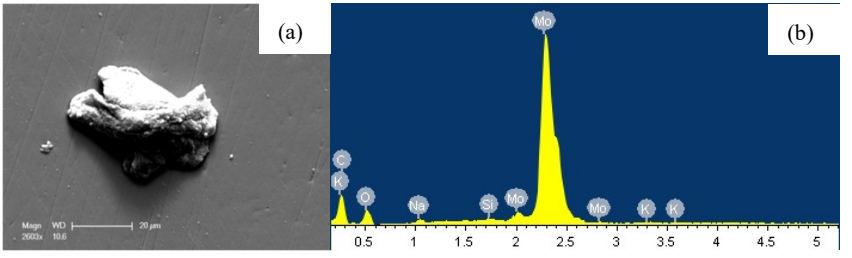

Fig. 5. (a) Particle adhering to the surface of the Mo grid generated by breakdown discharge (b) EDS spectrum of the particle.

The particle clusters were concentrated near the grid beam holes along with the pits and fallen debris, which could easily cause secondary breakdown discharge.

3.3. *Damage on the pyrolytic graphite grid*

Obvious holes on the surface of the PG grid after multiple ignitions can be seen in Fig. 6. After 300 ignitions, micrometer-scale layered fragments and fine cracks were visible on the PG grid surface, which indicated it had a layered structure like that shown in Fig. 6(a). After 500 ignitions, the extent of layered damage had increased. Pitting damage was observed, and the diameters of the pits reached 10 μm (Fig. 6(b)). After 1000 ignitions, the layers began to peel and generate debris. The pits were larger, and deep holes with sharp edges were visible (Fig. 6(c_3)).

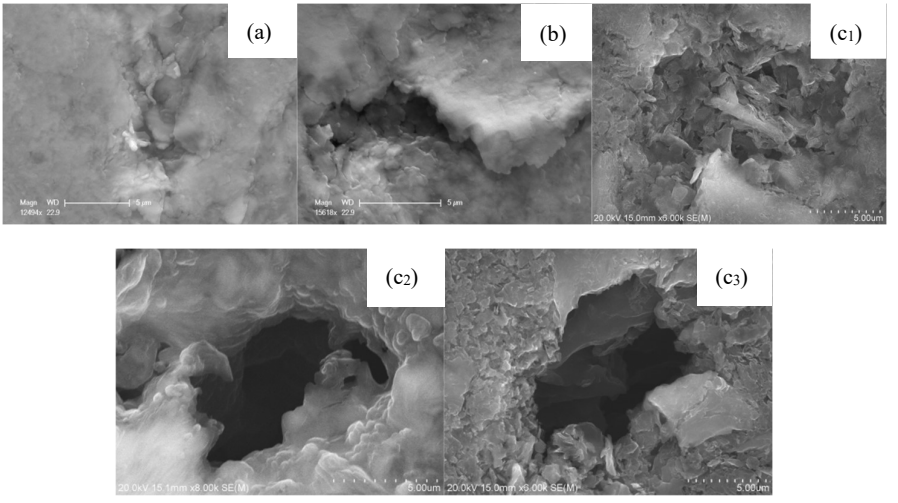

Fig. 6. The evolution of surface damage on the PG grid observed after (a) 300, (b) 500, (c) 1000 ignitions.

The damage was similar to the previously reported damage on a PG grid induced by breakdown under vacuum in a strong electric field.[17] This suggested that these features were formed by the same mechanism. The planar layered structure of the crystalline carbon and its low strength resulted in significant surface damage and failure of the material during breakdown discharge. The PG grid was prone to terrace-like damage during the breakdown discharge process, and the crystalline carbon sheets developed tipped edges. The terraced holes areas resembled the surface damage on the Mo grid. They were concentrated near the beam holes, which was the location affected by breakdown discharge in the ion optical system.

Several dozen microparticles like those observed on the Mo grid adhered to the PG grid near the beam holes. EDS analysis indicated that the composition of the particles was identical to that of PG, and carbon was the main component (Fig. 7). This suggested that the particles originated from the PG acceleration grid during the breakdown discharge. However, the pits on the PG grid were obviously large (>10 μm) than the pits on the Mo grid. This can be seen by comparing Figs. 4 and 6. Thus, the particles came primarily from the pits. Since the PG was composed of crystalline carbon layers, damage to the surface of the gird during breakdown discharge was inflicted layer by layer. The large particles mostly consisted of sheet-like structures. Particle clusters enhanced the local electric field in the ion optical system, which induced a subsequent breakdown discharge. The size of the damage area on the surface of the PG acceleration grid would thus increase, and even lead to thruster failure.

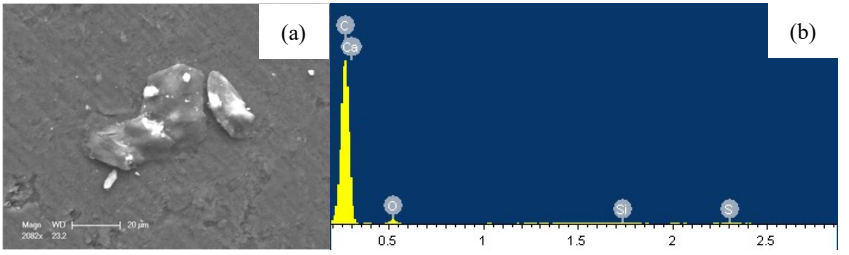

Fig. 7. (a) Layered debris on the surface on PG grid and (b) EDS analysis of a particle.

3.4. *Damage on the $Zr_{41.2}Ti_{13.8}Cu_{12.5}Ni_{10}Be_{22.2}$ alloy grid*

No serious damage was observed on the $Zr_{41.2}Ti_{13.8}Cu_{12.5}Ni_{10}Be_{22.2}$ alloy grid after 1000 ignitions (Fig. 8). Like in the Mo grid, small hemispherical impact pits near the alloy grid beam holes appeared after 300 ignitions (Fig. 8(a)). However, the small melt pits in Fig. 8(b) appeared on the alloy grid surface after 500 ignitions. This was the first obvious indication of melting. The molten pits were larger and more numerous after 1000 ignitions. The molten pits in Fig. 8(c_1) and Fig. 8(c_2). were clustered near the grid beam holes. A large molten pit with a lip can be seen in Fig. 8(c_1). The mechanism of pit lip formation was reported previously.[22] The shear stress on the surface of the material would be the lowest in the regions bombarded with particles and sputtering, and a lip would form around each pit. The center of the large melt pits was convex, and their diameter ranged from 2 to 5 μm. The lips on convex pits would enhance the local electric field and induce breakdown discharge between the grids.

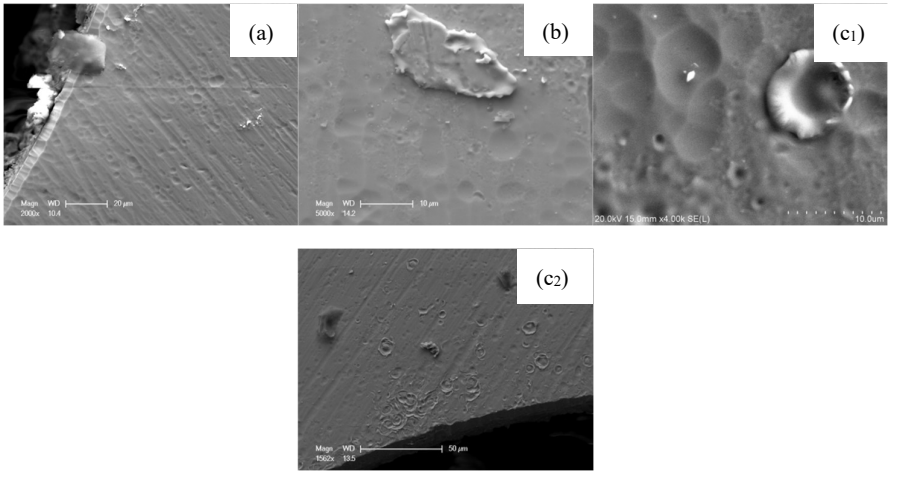

Fig. 8. The evolution of surface damage on the $Zr_{41.2}Ti_{13.8}Cu_{12.5}Ni_{10}Be_{22.2}$ alloy grid after (a) 300, (b) 500 and (c) 1000 ignitions.

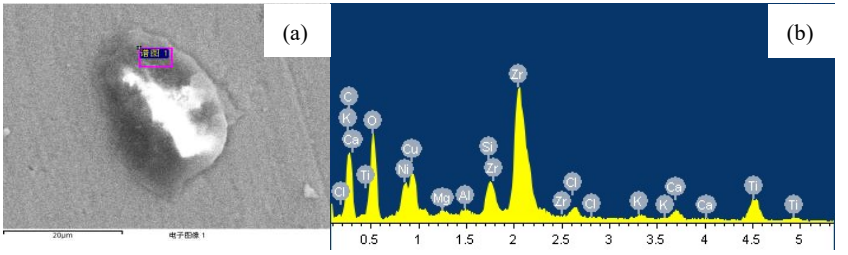

Fig. 9. (a) A molten particle on the surface of the alloy grid and (b) EDS spectrum of the particle.

The particles adhering to the surface of the alloy grid were composed of the same material used to make the acceleration gird. Like the particles on the Mo grid, the particles on the alloy grid were generated by melting. Most of the particles were distributed around the gird beam holes and formed in the breakdown discharge region (Fig. 9).

4. Discussion

The feasibility of the RIT ignition method based on Townsend discharge breakdown was verified experimentally. The threshold voltage V and the product of the distance d and gas pressure p between the grids followed Paschen's law. However, the surface of the acceleration grids exhibited damage once the number of ignitions reached certain threshold, and the damage would affect the lifetime of the thruster. Selection of an appropriate grid material is thus a key for extending the lifetime of the thruster.

Damage on the surfaces of the Mo, PG and $Zr_{41.2}Ti_{13.8}Cu_{12.5}Ni_{10}Be_{22.2}$ alloy μRIT-1 acceleration grids after multiple ignitions differed in appearance. Although Mo was fairly resistant to sputter corrosion, the most serious surface damage was observed on the Mo grid. Sinha[23] and Gooebel *et al*.[17] studied the surface damage on Mo electrodes caused breakdown discharge in a strong electric field under high vacuum. They found that the charged particles gained a large amount of energy in strong electric field and seriously damaged the surfaces of the grids. Bubble-like bulges and layered debris peeling from the Mo grid were observed in our experiment. The SEM images indicated that the Mo surface had a layered structure and contained gas. At the instant of breakdown discharge, a large number of high-energy particles bombarded the surface of the acceleration grid. Because of the short time of particle bombardment, the loss of heat due to conduction could be neglected.[22] High-energy particle bombardment increased the surface temperature of the Mo grid, and gas diffusion led to the formation of bubble-like structures. The damage due to bubble formation weakened the Mo surface and increased the local electric field, which induced secondary breakdown discharge between the grids. Continuous particle bombardment and temperature elevation caused the bubbles to burst, which generated debris. The remaining debris adhering to the grid surface generated a new and strong electric field, which likely induced tip discharge between grids.

The grids short-circuited when large amounts of debris were adhered to the insulator between them, and the thruster failed. On the basis of the damage on the Mo grid in Fig. 4(c), the ion optical system failed once the debris peeled from the grid surface. Grid short-circuiting is a hidden danger that can compromise the integrity of a propulsion system during subsequent thruster ignitions.

Some pitting damage due to breakdown discharge between the grids was observed on the surface of the PG grid, which was consistent with a previous report.[17] The layered structure of crystalline carbon and the low strength of PG made the material prone to failure. Terraced holes were generated by breakdown discharge and particle bombardment. The edges of the carbon layers formed tips, which triggered field emission or tip discharge. The large holes affected the lifetime of the ion optical system and the stability of the thruster. Subsequent ignitions gradually increased the size and the number of holes. The irregular shape of the acceleration grid surface would reduce the threshold voltage for ignition. In addition, the PG grid was less resistant to sputtering than the metal material. The beam holes in the PG grid were widened by ion beam sputtering, which adversely impacted thruster performance. On the basis of the RIT ignition method and the low resistance of PG to ion beam sputtering, PG was not a suitable grid material for the ion optical system.

The new alloy material, $Zr_{41.2}Ti_{13.8}Cu_{12.5}Ni_{10}Be_{22.2}$ was used to fabricate an RIT ion optical system grid for the first time in this study. Although the alloy was high in strength, was resistance to sputtering and exhibited few defects after repeated smelting at a high temperature, melt pits were visible on the alloy grid after multiple ignitions. The alloy had a relatively low melting point, because it contained copper (Table 1). The energy released during high-energy particle bombardment increased the temperature on the alloy surface. The surface of the grid melted and formed lipped pits. Although Shear stress during particle bombardment was lowest near the material surface, the energy of bombardment was not sufficient to completely destroy the material. Protrusions with diameters of 2–5 μm were observed in the center of the large melt pits.

The damage observed on the alloy grid after 1000 breakdown discharge would not cause the ion optical system to fail. However, melted areas on the alloy grid would gradually expand during subsequent ignitions. If a large number of melt pits formed around the gird beam holes, the electric field strength would increase rapidly. The threshold voltage of the grids would decrease, which would reduce thrust output and adversely affect performance.

5. Conclusion

This study provides a better insight into the feasibility of a new RIT ignition method based on Townsend discharge breakdown and the damages on the surface of acceleration grids made from different materials were evaluated. The main conclusions are as follows:

An ignition limit for each material on the basis of damage to the grid surface due to breakdown discharge. After 1000 ignitions, serious damage was observed on the surfaces of the Mo and PG grids. Once the ignition limit was exceeded, the damage would cause

the ion optical system to fail. Clusters of melt pits on the alloy grid caused by ignition had a limited effect on the stability of the thruster. However, a large number of melt pit clusters would reduce the threshold voltage for breakdown discharge, even under vacuum. The electric field between the girds during RIT ignition should be minimized. This will reduce the damage inflicted by high-energy particles and increase the lifetime of the ion optical system. However, the gas pressure pulse must be increased for ignition if the electric field is reduced. This will impact the attitude of the satellite, so the gas pressure pulse must be optimized for different space missions. The new ignition method based on Townsend discharge breakdown can be used to identify new and strong materials that are resistant to sputtering and high temperature to increase the lifetime of thrusters.

Acknowledgments

The author thanks for the alloy material support by Li Yansen, Ph.D. (Institute of Mechanics, CAS) and the financial support by the Strategic Priority Research Program of the Chinese Academy of Sciences under Grant Nos. XDB23030300, XDA1502070901 and XDA1502070503.

References

1. H. W. Loeb *et al*., Forty years of Giessen EP-activities and the recent RIT-microthruster development, *29th Int. Electric Propulsion Conf*. (Princeton, USA, 2005).
2. C. Collingwood, Investigation of a miniature differential ion thruster, dissertation, University of Southampton, School of Engineering Sciences (2011).
3. P. Hruby *et al*., Overview of Busek electric propulsion, *36th Int. Electric Propulsion Conf*. (Vienna, Austria, 2019).
4. M. Tsay *et al*., Micro radio-frequency ion propulsion system, *48th Joint Propulsion Conf*. (Atlanta, 2012).
5. T. A. Trudel, S. G. Bilén and M. M. Micci, Design and performance testing of a 1-cm miniature radio-frequency ion thruster, 3*1th Int. Electric Propulsion Conf*. (Ann Arbor, MI, 2009).
6. H. Watanabe *et al*., Experimental investigation of inductively coupled plasma cathode for the application to ion thrusters, *47th AIAA/ASME/SAE/ASEE Joint Propulsion Conf. Exhibit*. (California, 2013), pp. 127–140.
7. K. Hiramoto and Y. Takao, *Trans. Jpn. Soc. Aeronautical Space Sci. Aerospace Technol*. **14**, 57 (2016).
8. N. N. Antropov *et al*., *Thermal Eng*. **63**, 957 (2016).
9. J. W. He, Researchs on working mechanism and performance optimization of radio-frequency ion micro-thruster, dissertation, Institute of Mechanics, CAS (2017).
10. C.-C. Wu, X.-F. Sun, Z. Gu and Y.-H. Jia, *J. Propulsion Technol*. **40**, 232 (2019).
11. J. Cai *et al*., Study of radio-frequency ion micro-propulsion technology with iodide propellant, *14th China Electric Propulsion Conf*. (Changsha, 2018 in Chinese).
12. D. Feili *et al*., Performance mapping of new μN-RITs at Giessen, *29th Int. Electric Propulsion Conf*. (New Jersey, 2005).
13. H. Bassner, R. Killinger, H. Leiter and J. Muller, Development steps of the RF-Ion thrusters RIT, *27th Int. Electric Propulsion Conf*. (California, 2001).

14. T. Haruki, O. Takeshi and I. Kosuke, Plasma properties and ignition characteristics of RF ion source, *23th Int. Electric Propulsion Conf*. (Washington, 1993).
15. V. F. Mistoco, S. G. Bilen and M. M. Micci, Development and chamber testing of miniature radio-frequency ion thruster for microspacecraft, *40th AIAA/ASME/SAE/ASEE Joint Propulsion Conf. Exhibit*. (Florida, 2004).
16. A. Kuchler, *High Voltage Engineering Fundamentals· Technology· Applications* (Springer, 2017).
17. D. M. Goebel and A. C. Schneider, *IEEE Trans. Plasma Sci*. **33**, 1136 (2005).
18. J. Lu, G. Ravichandran and W. J. Johnson, *Acta Materialia*, **51**, 3429 (2003).
19. Y. S. Li *et al*., *J. Non-Crystalline Solids*. **513**, 76 (2019).
20. Y. L. Li *et al*., Dynamic tension mechanical properties research on $Zr_{41.2}Ti_{13.8}Cu_{12.5}Ni_{10}Be_{22.2}$ bulk metallic glass, *Int. Symp. Shock and Impact Dynamics,* 2011.
21. L. F. Ma, Study on performance optimization and ignition characteristics of micro radio frequency ion thruster, dissertation, Institute of Mechanics, CAS (2020).
22. M. M. Menon and K. D. Srivastava, *J. Appl. Phys*. **45**, 3832 (1974).
23. M. K. Sinha, Y. G. Ku and R. P. Johnson, *J. Appl. Phys*. **52**, 699 (1998).